ENHANCING THE MICROSTRUCTURE AND MECHANICAL PROPERTIES OF LOST FOAM CAST A356 ALLOY VIA ORBITAL SHAKING

Öznur Kılıç
Department of Metallurgical and Materials Engineering, Yildiz Technical University, Davutpasa Campus, Esenler, 34210 Istanbul, Turkey
TÜBİTAK Marmara Research Center (MAM), Barış Neighborhood. Dr. Zeki Acar Street. No: 1 P.K. 21, 41470 Gebze, Kocaeli, Turkey

Serhat Acar and Kerem Altuğ Güler
Department of Metallurgical and Materials Engineering, Yildiz Technical University, Davutpasa Campus, Esenler, 34210 Istanbul, Turkey

Copyright © 2026 The Author(s)
https://doi.org/10.1007/s40962-026-01995-3

Abstract

The mechanical performance of cast aluminum alloys is closely associated with their solidification microstructure, where a fine and homogeneous dendritic structure plays a critical role in achieving high strength and ductility. In this study, orbital shaking is investigated as a dynamic solidification control technique for refining the microstructure of A356 aluminum alloy produced by the lost foam casting (LFC) process. Casting experiments were carried out using expanded polystyrene (EPS) patterns at pouring temperatures of 720 °C and 780 °C. Orbital shaking speeds were varied between 50 and 200 rpm, and static castings were used as reference conditions. Microstructural characterization focused on the evaluation of secondary dendrite arm spacing (SDAS) and eutectic silicon morphology. The results show that low-to-moderate shaking intensities lead to a significant refinement in SDAS and improve material density by enhancing interdendritic feeding. At a pouring temperature of 720 °C, a shaking speed of 50 rpm reduced the SDAS from 91 to 65 µm, resulting in a marked increase in tensile strength from 141.4 to 172.4 MPa. In contrast, excessive shaking at 200 rpm caused microstructural coarsening and increased porosity, which are likely associated with intensified melt convection and altered feeding behavior in the semisolid state. Importantly, no visible coating damage or detachment was observed under the applied shaking conditions, indicating that orbital shaking does not induce mold-related defects such as penetration or cracking, which are commonly encountered in conventional mechanical vibration processes.

Keywords: *lost foam casting, A356 aluminum alloy, orbital shaking, dendritic refinement, microstructure*

Introduction

Aluminum and magnesium alloys are among the most significant engineering materials within the category of lightweight metals. In recent years, these alloys have found extensive applications in automotive manufacturing and the aerospace industry due to their ability to enhance energy efficiency. While each alloy group offers distinct advantages, their inherent properties sometimes make it difficult for a single alloy system to meet integrated performance requirements.[1,2] Among the advanced casting techniques, the lost foam casting (LFC) process offers notable advantages such as high casting precision, low production cost, and eco-friendliness, leading to its rapid global development.[3] In the Lost Foam Casting (LFC) process, patterns are predominantly fabricated from expanded polystyrene (EPS), polystyrene (PS), or polymethyl methacrylate (PMMA) polymers. These foam components are assembled into a single pattern or cluster, coated with a refractory slurry, and dried before being embedded in unbonded sand, which is compacted via

Received: 07 March 2026 / Accepted: 29 April 2026
Published online: 17 May 2026

vibration. Upon pouring, the thermal energy of the molten metal pyrolyzes the foam pattern, and the resulting gaseous decomposition products escape through the refractory coating into the sand. Consequently, the molten metal replaces the pattern, replicating its geometry. While widely adopted for aluminum automotive components, LFC is also extensively applied to various iron- and copper-based alloys.[4] EPS is commonly employed as the pattern material in the LFC process. In many applications, such as engine blocks, EPS patterns are bonded and assembled using a hot-melt adhesive with low thermal degradation due to their high dimensional accuracy.[5] As a near-net-shape technique, LFC offers distinct advantages by eliminating the need for binders and cores, thereby enabling the cost-effective production of highly complex geometries.[6] The use of unbonded sand, often coupled with vacuum assistance, facilitates the efficient removal of degradation gases while maintaining structural integrity against metallostatic pressure. However, the final quality of LFC components is highly sensitive to a complex interplay of process parameters, most notably the permeability of the mold and coating, gating system configuration, and pouring temperature.[7] Despite its operational benefits, LFC necessitates pouring temperatures typically 30–50 °C higher than conventional casting methods. This elevated thermal input, coupled with the low thermal conductivity of unbonded sand, inherently leads to sluggish solidification rates. Consequently, the resulting coarse grain structures tend to compromise the mechanical integrity of the components. Therefore, implementing grain refinement strategies is imperative to optimize the microstructural features and enhance the associated mechanical properties of LFC products.[8,9] Controlling the solidification microstructure remains a primary challenge in casting, as the goal is to achieve optimum mechanical performance at low cost and within shortened production cycles. Key desirable microstructural attributes include fine equiaxed grains, minimized microporosity, and enhanced resistance to hot cracking. Grain refinement can be achieved through post-solidification treatments such as heat treatment and rolling, or during solidification via rapid cooling, addition of grain refiners, or the application of dynamic effects such as vibration to the solidifying melt.[10] The efficacy of these methods in aluminum alloys is closely tied to the material's inherent metallurgical characteristics. In this specific context, the broad spectrum of quality requirements for aluminum alloys is governed by a complex interplay of parameters, including casting temperature, cooling rates, and porosity.[11] Kumar et al.[12] investigated the influence of mold vibration during the solidification of an Al–6%Cu alloy on its mechanical and microstructural properties. They observed that samples cast under vibration exhibited finer grains and superior mechanical performance, with increased vibration frequency resulting in further grain refinement and higher hardness values. Bustos et al.[13] investigated the rheological behavior of an A356 alloy during semisolid compression between parallel plates. The experiments utilized cylindrical specimens machined from billets solidified under a rotating permanent magnetic field. It was observed that the application of this magnetic field promoted melt stirring and shifted both dendritic and eutectic transformations toward lower temperatures, thereby enhancing microstructural refinement. Consequently, the resulting non-dendritic microstructure exhibited pseudoplastic flow behavior, characterized by a substantial increase in the load required to sustain deformation. Similarly, Shi et al.[14] applied ultrasonic treatment during the solidification of a 6016 aluminum alloy. Their findings indicated that ultrasonic vibration of the molten metal produced a completely refined and homogeneous microstructure. Wenming et al.[15] investigated the effects of vibration frequency on microstructure, mechanical properties, and fracture behavior of A356 aluminum alloy produced by expendable pattern shell casting using foam models. They reported improvements in density, yield strength, tensile strength, elongation, and hardness due to mechanical vibration.

Lastly, Wen-qi Zou et al.[16] studied the influence of vibration frequency on the microstructure and performance of high-chromium cast irons produced by LFC. They found that the microstructure in both non-vibrated and vibrated samples mainly consisted of primary carbides and eutectic colonies, but with increasing vibration frequency, the microstructure became noticeably finer.

In recent years, several studies have investigated the use of mechanical vibration, mold oscillation, and ultrasonic treatment during solidification to control the microstructure and mechanical properties of aluminum alloys. Kumar and Tewari[17] investigated the effect of mold oscillation during the solidification of A319 aluminum alloy. Their study demonstrated that oscillatory casting conditions promoted grain refinement and influenced the fracture characteristics of the alloy. The metallurgical behavior of the castings was evaluated through microstructural observations and mechanical testing, highlighting the influence of mold oscillation on the solidification behavior of the alloy. Mehta et al.[18] examined the influence of die vibration during the gravity die casting of Al-7Si-0.2Mg (A356) alloy. Their results indicated that die vibration significantly affected the microstructural evolution of the alloy and led to a reduction in secondary dendrite arm spacing (SDAS). The authors attributed this behavior to enhanced cooling conditions and forced convection generated by the die vibration during solidification. Ayar et al.[19] investigated the effect of mechanical vibration on the microstructure and mechanical properties of AlSi5Cu3 alloy. The results demonstrated that increasing vibration amplitude and duration promoted significant grain refinement. Correspondingly, improvements in hardness, tensile strength, and yield strength were observed compared to conventional casting conditions. Mu et al.[20] reported that ultrasonic vibration applied to the feeding channel during

solidification can enhance feeding efficiency and reduce shrinkage porosity in aluminum alloy castings, although excessive vibration intensity may diminish this beneficial effect. Kaya et al.[21] reported the production of A356 syntactic foams using vibration-assisted gravity die casting with recycled expanded glass spheres. Their results showed that vibration influenced the microstructural characteristics and the distribution of glass spheres within the foam structure. In addition, vibration-assisted casting led to improvements in the mechanical properties and corrosion resistance of the material.

Materials and Methods

The experimental procedure consisted of three main stages: mold preparation, melting and casting, and material characterization.

Mold Preparation

In the mold preparation stage, expanded polystyrene (EPS) sheets with a density of 10 kg/m^3 were selected as the pattern material. The EPS used in this study had a relatively low density and a correspondingly open bead structure, which is typical of EPS materials employed in experimental lost foam casting applications. An aluminosilicate-based refractory coating, typically used for EPS pattern applications in lost foam casting, was applied to the surface of the patterns as shown in Figure 1a. This coating was selected due to its high gas permeability and thermal stability. The coating can be applied by brushing, spraying, dipping, or flow coating. In the present study, the coating was applied to the EPC patterns by brushing. After application, the coated patterns were dried under room temperature conditions for approximately 24 h. To improve coating coverage, the application process was repeated once after drying. The coating thickness was approximately 0.2–0.3 mm. A micrograph showing the morphology of the refractory coating was presented in a previous study.[22]

The patterns, prepared in dimensions of 170 × 50 × 40 mm, were coated with the refractory coating and placed into a metal flask for molding. The experimental setup was intentionally simplified to provide a controlled framework for evaluating the influence of orbital shaking on solidification behavior. In this context, a simplified open-top pouring configuration was adopted to minimize additional variables associated with complex gating systems and to allow a more direct interaction between orbital motion and the advancing solidification front. To facilitate the molding process, the patterns were first positioned within the flask and surrounded by dry, unbonded silica sand with a grain fineness number (GFN) of approximately 45 AFS. This relatively coarse sand structure provides adequate permeability for the escape of gaseous decomposition products during the lost foam casting process. The sand was then compacted under vibration using an Octagon 200 (Endecotts Limited, UK) device to ensure uniform packing. At the final stage of mold preparation, a feeder sleeve with a height of 10 mm was placed on top of the pouring basin.

Orbital motion during solidification was provided using a custom-built Mikrotest orbital shaker. The prepared molds were placed on the shaker platform. Orbital shaking was initiated during the pouring of the molten metal and maintained throughout the solidification stage. The duration of orbital shaking corresponded to the total solidification time, which was approximately 90–120 s depending on the pouring temperature. The shaking rate was adjusted and monitored in terms of rotational speed (rpm) using the digital control panel of the device. Photographs of the molding setup and orbital shaking system are presented in Figure 1b and c.

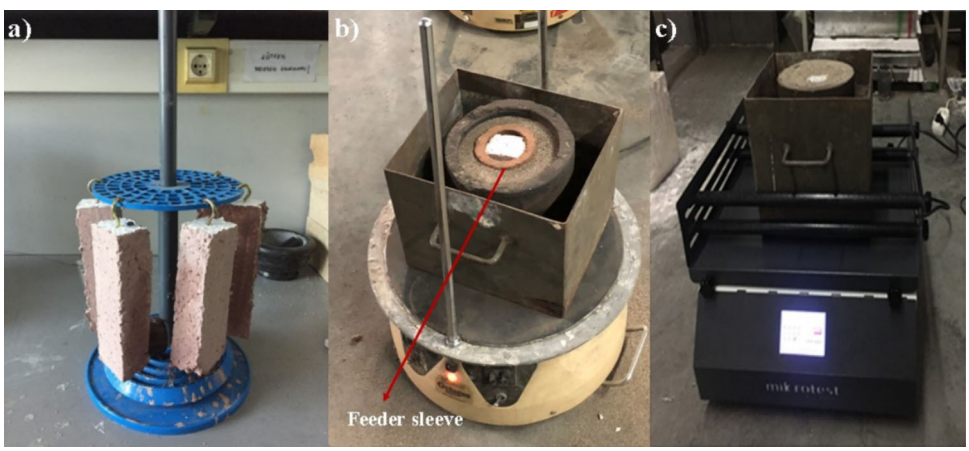


Figure 1. (a) Models prepared with refractory coating (b) Vibration device used during the molding process (c) The orbital shaking apparatus employed during the casting process

Melting and Casting

A356 aluminum alloy ingots were sectioned into charges weighing between 1.00 and 1.20 kg and subsequently melted in clay–graphite crucibles (Size A4). The chemical composition of the A356 alloy used in this study is presented in Table 1.

Melting was conducted in an electric resistance furnace, with pouring temperatures set at 720 °C and 780 °C. These relatively high pouring temperatures were intentionally selected to extend the solidification duration, thereby enhancing the interaction between melt convection and the advancing solidification front. This approach enables orbital shaking to more effectively influence dendritic evolution during solidification. As shown in Figure 2, castings were conducted under static and orbital shaking conditions at speeds of 50, 100, 150, and 200 rpm.

Material Characterization

Specimens were sectioned from the cast components using a precision cutting machine equipped with a diamond disk. To evaluate possible microstructural variations, samples were extracted from the initial solidification zones as well as from the central and peripheral regions of the castings.

Metallographic preparation was carried out through sequential grinding using silicon carbide (SiC) abrasive papers (320–2000 grit), followed by final polishing with a 1-μm diamond suspension. The polished surfaces were then etched with Keller's reagent for approximately 60 s to reveal the microstructure. Microstructural examinations were performed using optical microscopy for both qualitative observation and quantitative analysis. The quantitative analysis included measurements of secondary dendrite arm spacing (SDAS) and eutectic silicon aspect ratio (length-to-width). SDAS values were determined by averaging measurements taken from multiple regions of each specimen. Mechanical properties were evaluated using Brinell hardness testing with a 2.5 mm diameter steel ball under a load of 62.5 kgf. The density of the samples was measured based on Archimedes' principle using an analytical balance equipped with a density determination kit. Tensile and impact tests were conducted to assess the effect of processing parameters on mechanical performance. Tensile testing provided yield strength, ultimate tensile strength, and elongation at fracture. Impact toughness was evaluated using V-notched specimens in accordance with the Charpy impact testing method.

Result and Discussion

Castings were produced using foam patterns with a density of 10 kg/m^3 at pouring temperatures of 720 °C and 780 °C. The experiments were conducted under both static conditions and orbital shaking at rotational speeds of 50, 100, 150, and 200 rpm. To evaluate the combined effects of pouring temperature and shaking intensity on microstructural evolution, specimens were extracted from different regions of the castings for characterization. For each condition, microstructural analyses were performed on samples taken from both the central and peripheral regions, as schematically illustrated in Figure 3.

Following casting, macrostructural inspection revealed no visible defects and confirmed high dimensional fidelity to the original foam patterns. Although dimensional accuracy was not quantitatively evaluated in this study, no visually observable distortion or dimensional inconsistency was detected in the produced castings under the investigated shaking conditions. The microstructures of samples obtained from both central and peripheral regions at pouring temperatures of 720 °C and 780 °C are presented in Figures 4 and 5. All specimens exhibited a typical hypoeutectic Al-Si microstructure, characterized by light-gray primary α-Al dendrites and dark, acicular eutectic silicon phases.

Microstructural refinement under dynamic conditions was associated with modifications in dendritic morphology during solidification. Orbital shaking contributed to this refinement by influencing dendrite growth behavior and improving structural uniformity. The induced centrifugal forces generated shear stresses at the solidification front, which affected the evolution of the primary α-Al phase. No significant differences were observed between the central and peripheral regions in terms of microstructural characteristics.

Secondary dendrite arm spacing (SDAS) and eutectic silicon aspect ratio values for all casting conditions are summarized in Tables 2 and 3. Figure 6 illustrates the correlation between shaking speed and SDAS. For the 720 °C pouring temperature, the initial SDAS values in both the peripheral and central regions under static conditions were approximately 90 μm. Upon the application of

Table 1. Chemical Composition of A356 Aluminum Alloy (wt%)[23]

Al	Si	Mg	Fe	Ti	Pb	Cu	Mn	Cr	Ni
Balance	7.28	0.35	0.14	0.12	0.011	0.01	0.02	0.003	0.003

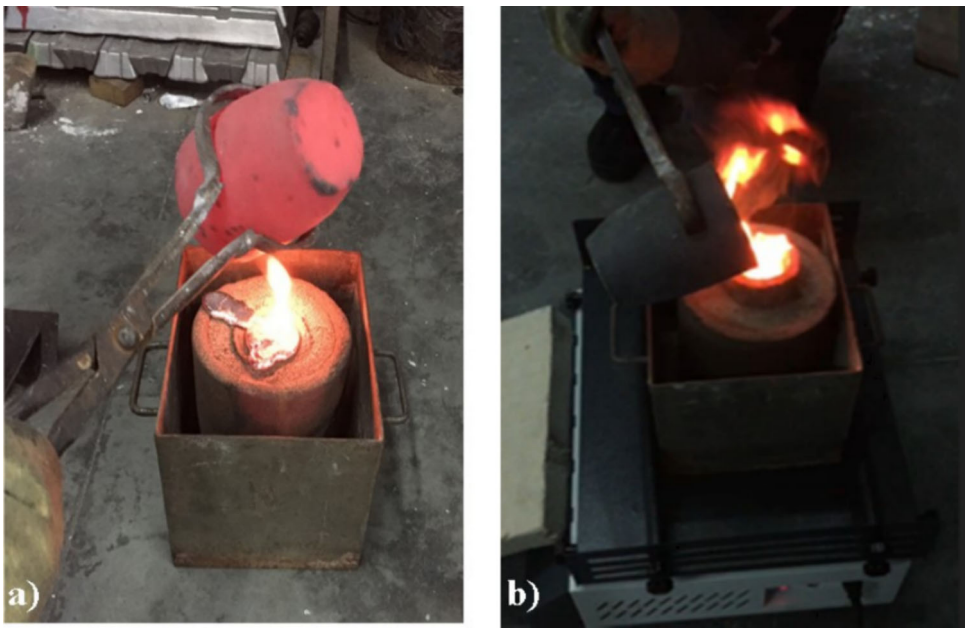


Figure 2. (a) Casting process carried out without orbital shaking (b) The casting process carried out with orbital shaking

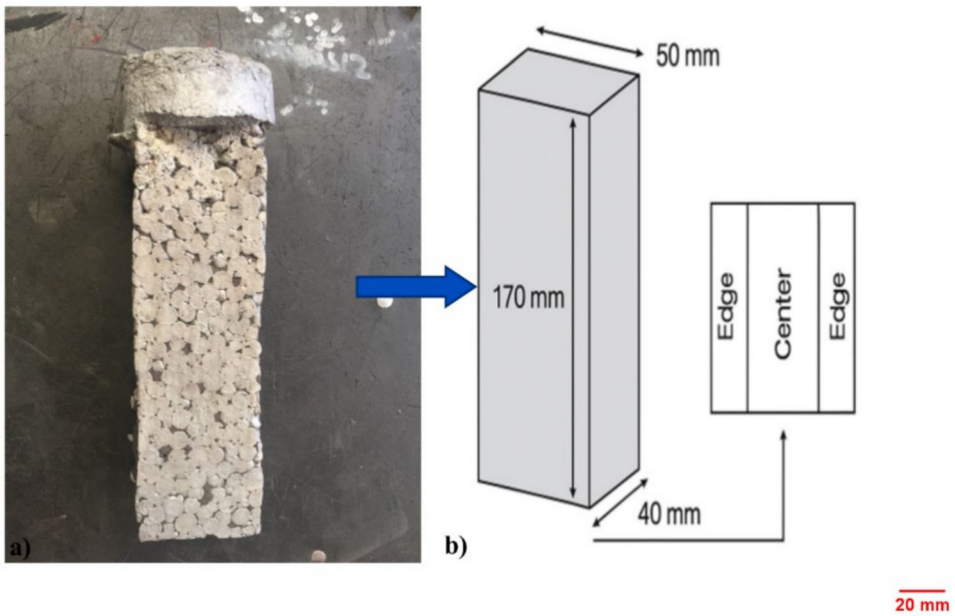


Figure 3. (a) Photograph of a representative as-cast part, (b) schematic illustration of the casting sample geometry and sampling locations

orbital shaking, SDAS decreased significantly before reaching a plateau at higher speeds. While the induced centrifugal force was sufficient to promote a rosette-like dendritic morphology, it proved insufficient to sustain further refinement at elevated shaking intensities. The cessation of refinement at 200 rpm may be associated with the interaction and coalescence of partially solidified dendritic structures or localized remelting effects during the semisolid stage, both of which could reduce the effectiveness of dendritic refinement.

In contrast, specimens cast at 780 °C exhibited higher initial SDAS values (approximately 100 μm) under static conditions. The reduction in SDAS with shaking was gradual rather than abrupt, and the values remained relatively stable across the speed range. The minimum SDAS at 780 °C was achieved at 150 rpm; however, a slight increase in SDAS was observed at 200 rpm, consistent with the coarsening trend observed in the 720 °C series.

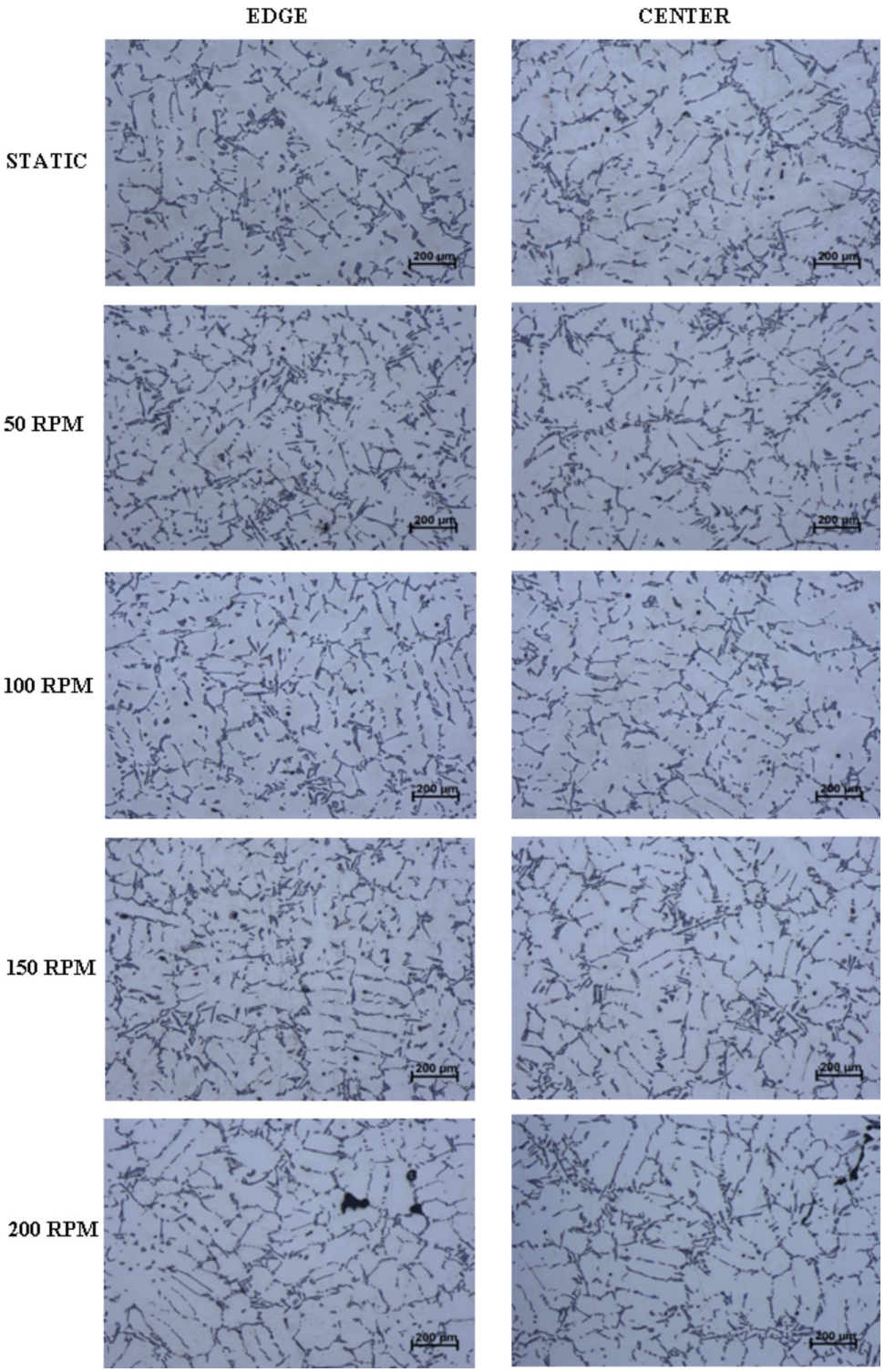


Figure 4. Microstructure images of casting at 720 °C (50x)

The reduction in SDAS with increasing shaking intensity is commonly attributed to enhanced melt convection and dendrite arm fragmentation during solidification. Orbital shaking promotes fluid flow in the semisolid region, disrupting dendrite growth and leading to a finer microstructure. However, at higher shaking intensities, excessive convection may destabilize the solidification front, promoting dendrite coalescence and localized remelting. This behavior explains the limited refinement and the onset of coarsening observed at 200 rpm.

The effect of shaking intensity on eutectic silicon morphology was evaluated using aspect ratio measurements, defined as the mean ratio of particle length to width. This

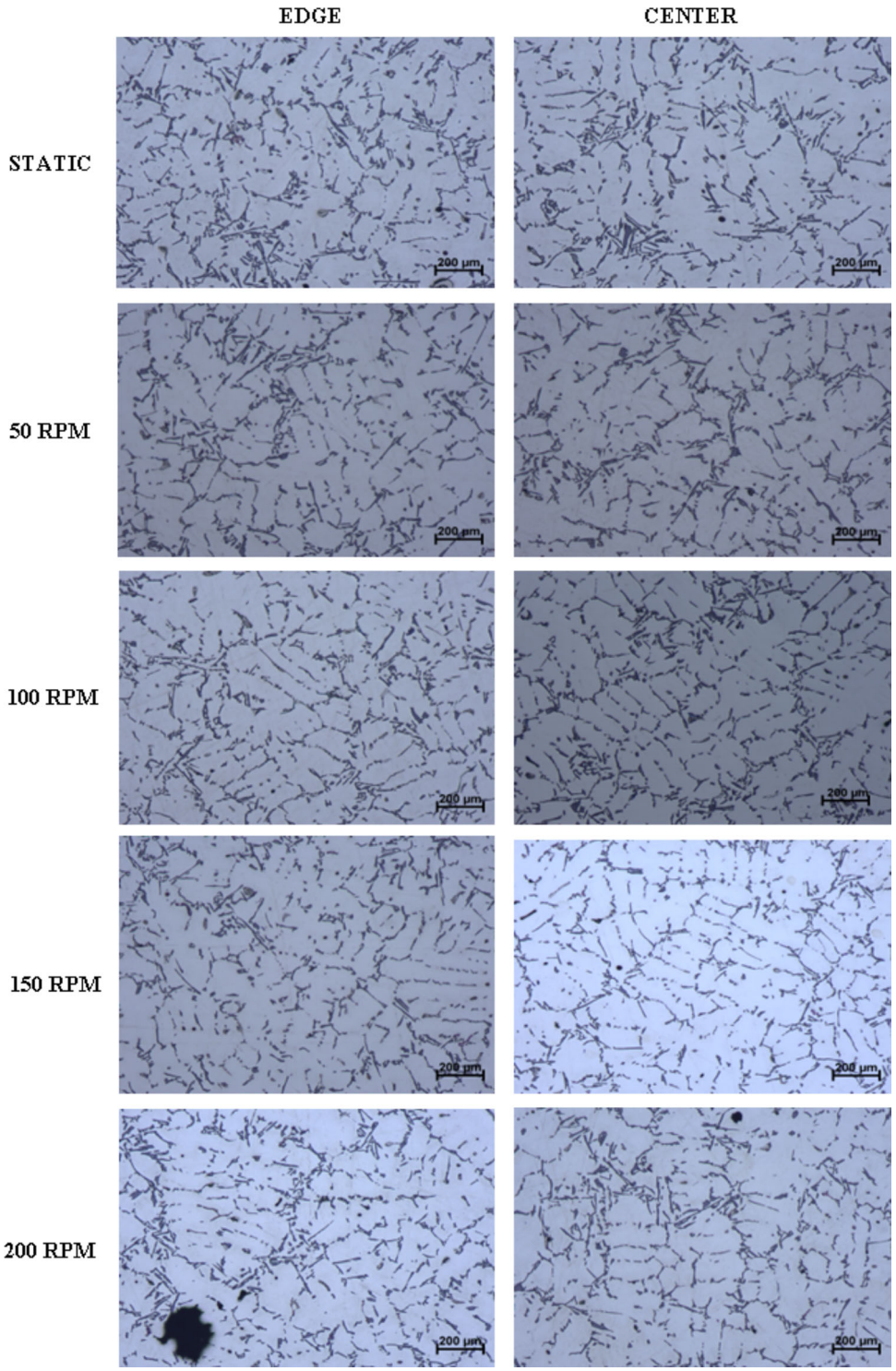


Figure 5. Microstructure images of casting at 780 °C (50x)

parameter serves as a quantitative indicator of the fragmentation degree of the typically plate-like silicon structures. Measurements were conducted across multiple regions, encompassing both the peripheral and central areas of each specimen, and the reported values represent the overall mean.

As illustrated in Figure 7a for specimens cast at 720 °C, the aspect ratio under static conditions was approximately 10 in both the peripheral and central regions. At low shaking speeds, this value decreased significantly to approximately 5, indicating substantial fragmentation and partial spheroidization of the eutectic silicon plates. However, as

Table 2. SDAS, Length/Width Ratio of Samples Casted at 720 °C

	SDAS (720°C)		Length/Width (720°C)	
	Edge	Center	Edge	Center
Static	91±3.3	91±5.6	10.6±1.2	9.3±0.9
50 rpm	63±2.2	67±2	7.4±0.9	6.9±0.7
100 rpm	74±2.4	70±2.2	6.4±0.6	5.2±0.6
150 rpm	65±2.1	74±2.4	11±0.9	10.1±0.8
200 rpm	75±2.7	73±2.6	11.4±1.1	13.1±0.8

Table 3. SDAS, Length/Width Ratio of Samples Casted at 780 °C

	SDAS (780 °C)		Length/Width (780 °C)	
	Edge	Center	Edge	Center
Static	98±4.8	100±3.7	11.6±1.3	10.6±1
50 rpm	89±3.1	92±2.1	6.8±1	6.6±0.9
100 rpm	78±2.3	81±2.3	4.7±0.4	3.8±0.4
150 rpm	74±2.4	75±1.9	12.5±1	11.8±2.9
200 rpm	89±2.6	84±4.7	10.1±0.8	11.9±0.9

the shaking intensity increased to moderate and high levels, the aspect ratio rose, approaching the initial static-casting values. A similar trend was observed for specimens cast at 780 °C (Figure 7b), where the aspect ratio decreased from approximately 10 to about 4 at low speeds but returned to nearly 10 at higher intensities.

These comparative results demonstrate that low-intensity agitation positively influences the spheroidization of eutectic silicon at both temperatures by promoting the break-up of elongated morphologies. Conversely, moderate-to-high intensities appear less effective, possibly due to enhanced melt turbulence that may alter the stability or orientation of fragmented silicon particles. Notably, the reduction in aspect ratio at low speeds was slightly more pronounced at 720 °C, suggesting that the relatively faster solidification at the lower pouring temperature may preserve the modified morphology more effectively before reconfiguration occurs.

The observed modification in eutectic silicon morphology is commonly attributed to the enhanced melt flow and shear forces induced by orbital shaking. These effects promote the fragmentation of plate-like silicon structures and their partial spheroidization during solidification. From a microstructural perspective, elongated silicon particles tend

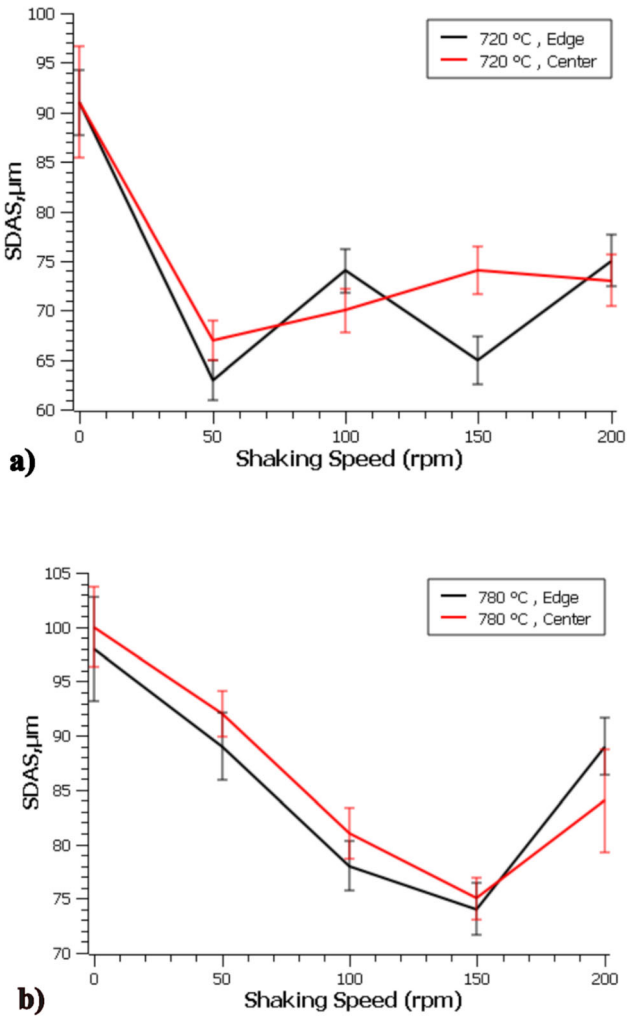


Figure 6. Effect of shaking speed on SDAS in specimens cast at 720 °C (a) and 780 °C (b)

to maintain their anisotropic morphology, whereas fragmented and more rounded particles exhibit a more uniform distribution within the matrix. However, at higher shaking intensities, increased turbulence may lead to the realignment or coarsening of silicon particles, limiting the effectiveness of morphological modification.

The hardness values for the specimens cast at 720 °C and 780 °C are presented in Table 4. In this study, mechanical tests were conducted on specimens in the as-cast (F condition) state in order to isolate the effect of orbital shaking during solidification without the influence of post-casting heat treatments.

Under static conditions, the secondary dendrite arm spacing (SDAS) was approximately 90 µm at 720 °C and about 100 µm at 780 °C. The pronounced reduction in SDAS at low shaking intensities was accompanied by a corresponding increase in hardness at both temperatures. This improvement is likely associated with dendritic refinement and improved melt feeding behavior, which may contribute

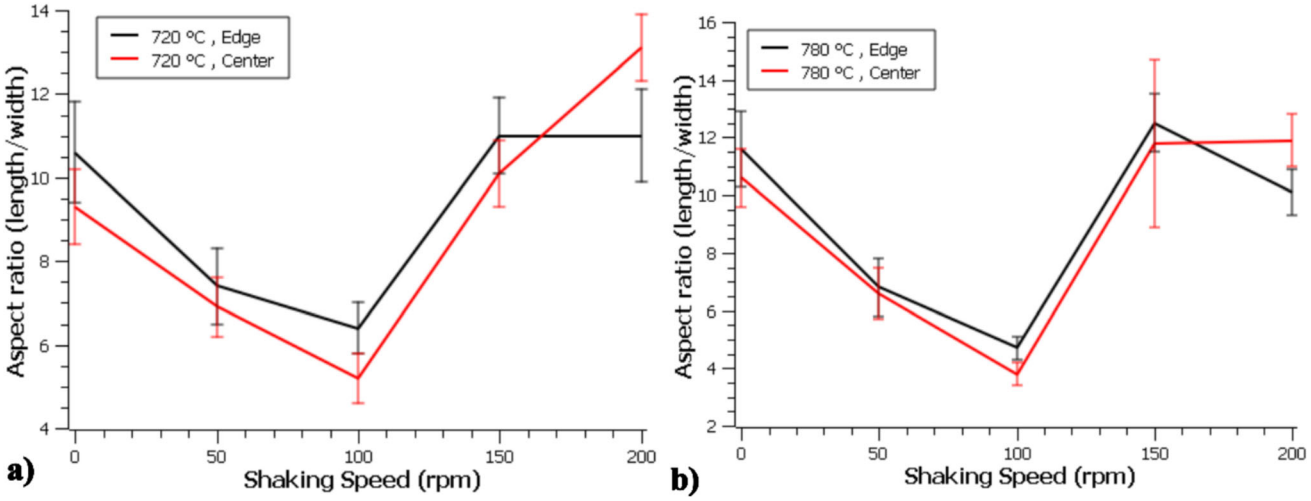


Figure 7. Effect of shaking speed on aspect ratio (length/width) of eutectic silicon at 720 °C (a) and 780 °C (b)

Table 4. Hardness Values of the Specimens Cast at 720 °C and 780 °C

Shaking speed	Hardness (HB) 720 °C Edge	Hardness (HB) 720 °C Center	Hardness (HB) 780 °C Edge	Hardness (HB) 780 °C Center
Static	55±2.60	55±3.13	56±2.45	56±3.05
50 rpm	68±3.13	66±3.37	68±3.47	67±3.70
100 rpm	57±2.54	56±2.68	57±2.25	56±2.45
150 rpm	62±1.94	59±2.62	63±3.04	60±2.44
200 rpm	60±4.39	57±5.42	61±4.09	58±5.04

to reduced interdendritic microporosity and enhanced load-bearing capacity.

At moderate shaking speeds, hardness values remained relatively stable, consistent with the comparable SDAS values observed within this processing window. However, at a high shaking speed of 200 rpm, an increase in SDAS was recorded alongside a reduction in density. This behavior suggests that excessive agitation may disturb the solidification–feeding balance, potentially increasing porosity and thereby reducing hardness.

Overall, the comparative analysis indicates that for both temperature regimes, low-to-moderate shaking speeds promote favorable microstructural evolution and feeding conditions, resulting in improved hardness. In contrast, excessive shaking intensity appears to diminish these benefits by coarsening dendritic features and negatively influencing feeding efficiency.

To further evaluate the influence of shaking speed and casting temperature on mechanical behavior, the specimens were subjected to tensile and Charpy impact testing. The results for specimens cast at 720 °C and 780 °C are summarized in Tables 5 and 6, respectively. The density values are presented alongside the mechanical test results in the same tables, enabling a direct evaluation of the relationship between density and mechanical performance.

A consistent trend was observed for the specimens cast at 720 °C (Table 5). The static condition exhibited the lowest density (2.57 g/cm^3). A slight increase in density was observed at 50 rpm; however, further increases in shaking intensity led to a gradual decrease, with the density at 200 rpm approaching that of the static condition. This behavior suggests that moderate agitation may contribute to improved melt flow and interdendritic feeding, potentially reducing microporosity, whereas excessive turbulence may adversely affect feeding efficiency. Nevertheless, a one-way analysis of variance (ANOVA) indicated that the effect of shaking speed on density at 720 °C was not statistically significant (p = 0.997), indicating that orbital shaking does not result in a measurable change in bulk density under the investigated conditions.

Consistent with the hardness profiles, the pronounced reduction in secondary dendrite arm spacing (SDAS)—accompanied by overall microstructural refinement—was associated with improved tensile properties at low-to-moderate shaking speeds. For instance, the ultimate tensile strength (UTS) increased from 141 MPa under static conditions to approximately 170 MPa under optimized shaking parameters. Within this low-to-moderate range, the mechanical properties exhibited a relatively stable plateau. However, increasing the shaking speed to 200 rpm resulted in an increase in SDAS and slight variations in density, corresponding to lower tensile performance. This behavior may be related to reduced feeding efficiency and increased porosity under excessive agitation, which negatively influenced overall mechanical integrity.

Table 5. Tensile properties, Charpy Impact Energy Results, and Density Values of Samples Cast at 720 °C

Sample	Yield strength (MPa)	Tensile strength (MPa)	Elongation %	Impact toughness (J/cm^2)	Density g/cm^3
Static	124.5±0.9	141.4±1.1	2.70±0.2	1.99±0.3	2.57±0.3
50 rpm	126.9±0.9	172.4±1.0	4.90±0.3	2.2±0.1	2.64±0.3
100 rpm	130.7±1.3	167.4±1.5	2.70±0.4	2.24±0.1	2.63±0.1
150 rpm	123.1±0.8	155.2±1.0	3.40±0.2	2.1±0.1	2.61±0.2
200 rpm	85.4±1.2	98.4±1.5	1.50±0.3	1.91±0.1	2.59±0.3

Table 6. Tensile Properties, Charpy Impact Energy Results, and Density Values of Samples Cast at 780 °C

Sample	Yield strength (MPa)	Tensile strength (MPa)	Elongation (%)	Impact toughness (J/cm^2)	Density g/cm^3
Static	115.6±1.2	131.8±1.5	1.3±0.3	2±0.1	2.58±0.2
50 rpm	132.8±1.1	153.6±1.4	4.4±0.2	2.11±0.1	2.61±0.1
100 rpm	128.1±0.9	159.9±1	4.3±0.4	1.98±0.1	2.64±0.1
150 rpm	127.1±0.5	140.8±0.8	2.9±0.3	1.9±0.1	2.65±0.3
200 rpm	123.6±1.2	132.6±1.4	1.4±0.3	1.95±0.1	2.59±0.3

In contrast, the Charpy impact tests yielded toughness values ranging from 1.91 to 2.24 J/cm^2. Although minor variations were observed among the different shaking conditions, the overall change in impact toughness remained relatively limited compared to the variations in tensile properties. These results suggest that while dynamic agitation significantly influences microstructural evolution and enhances tensile strength, its effect on fracture behavior and energy absorption capacity is comparatively less pronounced within the investigated parameter range.

The one-way ANOVA was conducted to assess the statistical significance of the mechanical property variations under different shaking conditions. The analysis demonstrated that the effects of shaking speed on yield strength ($p = 7.30 \times 10^{-13}$), ultimate tensile strength ($p = 3.94 \times 10^{-14}$), and elongation ($p = 8.77 \times 10^{-7}$) were statistically highly significant ($p < 0.05$). Among these, tensile strength exhibited the most pronounced response to orbital shaking. In contrast, the variation in impact toughness was not statistically significant ($p = 0.139$), indicating a lower sensitivity to the applied processing conditions.

The density values of the specimens cast at 780 °C are presented in Table 6. The static condition exhibited the lowest density (2.58 g/cm^3). A slight increase in density was observed with increasing shaking intensity; however, the specimen processed at 200 rpm showed a density comparable to that of the static condition, indicating that excessive agitation does not promote further densification. This behavior suggests that low-to-moderate shaking intensities may enhance interdendritic melt feeding and reduce microporosity, whereas excessive turbulence may disrupt solidification dynamics and decrease feeding efficiency. According to the one-way ANOVA results statistical significance of density variations under different shaking conditions, the results indicated that the effect of shaking speed on density at 780 °C was not statistically significant ($p = 0.993$), suggesting that orbital shaking does not produce a measurable change in bulk density within the investigated parameter range.

Consistent with the hardness results, the reduction in secondary dendrite arm spacing (SDAS) was associated with improved mechanical performance at low-to-moderate shaking speeds compared with static casting. For example, at 780 °C, the tensile strength increased from 131 MPa under static conditions to approximately 160 MPa under optimal shaking. Within this shaking speed range, the tensile properties remained relatively close to one another, reflecting comparable SDAS values. However, at a high shaking speed of 200 rpm, the increase in SDAS combined with reduced feeding efficiency during solidification was associated with increased porosity, which corresponded to lower mechanical performance.

Charpy impact test results revealed toughness values ranging from 1.95 to 2.00 J/cm^2, indicating that shaking had a limited influence on impact resistance. These findings suggest that while controlled shaking enhances tensile performance through dendritic refinement and improved feeding behavior, its effect on impact toughness remains minimal within the investigated processing window.

The one-way ANOVA revealed that the effects of shaking speed on yield strength ($p = 2.12 \times 10^{-8}$), ultimate tensile strength ($p = 2.14 \times 10^{-10}$), and elongation ($p = 2.50 \times 10^{-7}$) were statistically highly significant ($p < 0.05$). In contrast, the variation in impact toughness was not statistically significant ($p = 0.201$), indicating a lower sensitivity to the applied shaking conditions. Among the investigated properties, tensile strength exhibited the most pronounced response to orbital shaking.

The observed improvements in mechanical properties are commonly attributed to the combined effects of dendritic refinement, eutectic silicon modification, and reduced microporosity. At 720 °C, the pronounced reduction in SDAS and the more effective fragmentation of eutectic silicon contribute to a more homogeneous microstructure, enhancing load transfer and promoting improved tensile strength and elongation. In addition, the relatively faster solidification conditions at this temperature help preserve the refined microstructural features, leading to a more efficient interdendritic feeding behavior and a reduction in microvoid formation.

At 780 °C, although similar trends are observed, the higher pouring temperature results in slower solidification kinetics, which limits the effectiveness of dendritic refinement and silicon modification. As a result, the improvement in mechanical properties is comparatively less pronounced. Furthermore, the wider semisolid interval at elevated temperatures may reduce the stability of the refined structures, allowing partial coarsening or reconfiguration during solidification.

However, at higher shaking intensities (200 rpm), the coarsening of dendritic structures combined with reduced feeding efficiency leads to increased microporosity, which negatively affects mechanical performance. This indicates that while orbital shaking enhances microstructural control within an optimal processing window, excessive agitation disrupts the solidification–feeding balance and diminishes the overall mechanical benefits.

Conclusion

The present study demonstrates that orbital shaking provides an effective and controllable dynamic microstructural refinement strategy for Al-Si alloys produced by lost foam casting. A pronounced reduction in secondary dendrite arm spacing (SDAS) was achieved at 720 °C, decreasing from 91 μm under static conditions to 65 μm at 50 rpm. This refinement was accompanied by a noticeable improvement in mechanical performance, with tensile strength increasing from 141 to 172 MPa and elongation improving from 2.7 to 4.9%. A similar trend was observed at 780 °C, although the refinement effect was comparatively less pronounced. Under optimal shaking conditions, the tensile strength increased from 131 MPa in the static condition to approximately 160 MPa, while elongation improved from 1.3% to around 4.3%. These results highlight the combined influence of thermal conditions and agitation intensity on microstructural evolution and mechanical performance.

Dendritic refinement and feeding performance were optimized within a low-to-moderate shaking range (50–150 rpm). However, beyond this range, further increases in shaking intensity led to a deterioration in microstructural characteristics. At high shaking speeds (200 rpm), an increase in SDAS was observed, indicating dendritic coarsening. This coarsening was directly reflected in mechanical performance, with tensile strength decreasing to approximately 98 MPa and elongation dropping to around 1.5% at 720 °C. A similar trend was observed at 780 °C, where tensile strength decreased to approximately 132 MPa and elongation to around 1.4% at 200 rpm. This behavior was accompanied by slight variations in density, decreasing from approximately 2.58 g/cm^3 in the static condition to values close to 2.57 g/cm^3 at high shaking intensity. However, these changes were not statistically significant and remain within experimental scatter. This suggests that excessive agitation may influence solidification–feeding conditions; however, its effect on bulk density remains limited. Enhanced melt convection and heat redistribution at high intensities may alter local cooling conditions, potentially reducing the effectiveness of refinement.

The inherent mold-filling mechanism of lost foam casting promotes directional solidification through the development of a reverse temperature gradient as the advancing melt decomposes the foam pattern. High-intensity shaking may disrupt this solidification–feeding balance, while metal spillage at elevated speeds could reduce metallostatic pressure and feeding efficiency.

Importantly, orbital shaking enabled microstructural control without visible coating damage under the applied conditions, unlike conventional mechanical vibration. Therefore, orbital shaking represents a mechanically non-destructive and process-compatible refinement approach for lost foam casting, with potential applicability to other foundry systems where coating stability and controlled solidification are critical.

Funding

Open access funding provided by the Scientific and Technological Research Council of Türkiye (TÜBITAK).

Conflict of interest On behalf of all authors, the corresponding author states that there is no conflict of interest.

Open Access

This article is licensed under a Creative Commons Attribution 4.0 International License, which permits use, sharing, adaptation, distribution and reproduction in any medium or format, as long as you give appropriate credit to the original author(s) and the source, provide a link to the Creative Commons licence, and indicate if changes were made. The images or other third party material in this article are included in the article's Creative Commons licence, unless indicated otherwise in a credit line to the material. If material is not included in the article's Creative Commons licence and your intended use is not permitted by statutory regulation or exceeds the permitted use, you will need to obtain permission directly from the copyright holder. To view a copy of this licence, visit http://creativecommons.org/licenses/by/4.0/.

REFERENCES

1. G. Li, W. Jiang, Z. Fan, Z. Jiang, X. Liu, F. Liu, Effects of pouring temperature on microstructure, mechanical properties, and fracture behavior of Al/Mg bimetallic composites produced by lost foam casting process. Int. J. Adv. Manuf. Technol. **91**, 1355–1368 (2017). https://doi.org/10.1007/s00170-016-9810-y
2. G.Y. Li, F. Guan, W.M. Jiang, Y.C. Xu, Z. Zhang, Z.T. Fan, Effects of mechanical vibration on filling and solidification behavior, microstructure and performance of Al/Mg bimetal by lost foam compound casting. China Foundry **20**, 469–479 (2023). https://doi.org/10.1007/s41230-023-2168-5
3. M.C. Poletti et al., Effect of lost-foam casting process on properties of spiral blade. Crystals **12**, 1075 (2022). https://doi.org/10.3390/cryst12081075
4. K. Siavashi, The effect of casting parameters on the fluidity and porosity of aluminium alloys in the lost foam casting process. Doctoral thesis, Faculty of Engineering (1988).
5. K. Bieniewicz, M. Reich, N. Soraruf, A. Steer, P. Sanders, J. Belke, Improving metal flow in lost foam casting through use of low thermal degradation hot melt adhesives. Inter Metalcast (2025). https://doi.org/10.1007/s40962-024-01331-7
6. K. Fedorov, G. Stoyanov, N. Sydorenko, C.R. Ravindran, K. Fayazbakhsh, Evaluation of 3D printed foam patterns for hybrid lost foam casting of A356 alloy. J. Manuf. Process. **126**, 429–442 (2024). https://doi.org/10.1016/j.jmapro.2024.07.080
7. K. Paramasivam, M.V. Anand, M. Sambathkumar, Investigation of optimum process parameter of lost foam casting of A356/SiC metal matrix composite. Mater. Today Proc. **47**, 4801–4806 (2021). https://doi.org/10.1016/j.matpr.2021.06.035
8. I. Tutuk, S. Acar, K.A. Guler, The application of the direct water cooling process on the lost-foam casting technique to improve microstructural and mechanical properties of A356 alloy. Int. J. Metalcast. **17**, 2324–2337 (2023). https://doi.org/10.1007/s40962-022-00950-2
9. B. Xiao, Z. Fan, W. Jiang, X. Liu, W. Long, Q. Hu, Microstructure and mechanical properties of ductile cast iron in lost foam casting with vibration. J. Iron. Steel Res. Int. **21**, 1049–1054 (2014). https://doi.org/10.1016/s1006-706x(14)60182-5
10. N. Abu-Dheir, M. Khraisheh, K. Saito, A. Male, Silicon morphology modification in the eutectic Al–Si alloy using mechanical mold vibration. Mater. Sci. Eng. A **393**, 109–117 (2005). https://doi.org/10.1016/j.msea.2004.09.038
11. Ö. Yalçin, M. Çolak, Investigation of the effect of niobium addition on fluidity and mechanical properties in casting of aluminum alloys. Int. J. Metalcast. (2025). https://doi.org/10.1007/s40962-025-01613-8
12. R. Kumar, M. Salim Ansari, S. Sekhar Mishra, A. Kumar, Effect of mould vibration on microstructure and mechanical properties of casting during solidification. Int. J. Eng. Res. Technol. (IJERT) **3**, 90 (2014)
13. O. Bustos, S. Ordonez, R. Colas, Rheological and microstructural study of A356 alloy solidified under magnetic stirring. Int. J. Metalcast. **7**, 29–37 (2013). https://doi.org/10.1007/bf03355542
14. C. Shi, K. Shen, D. Mao, Y. Zhou, F. Li, Effects of ultrasonic treatment on microstructure and mechanical properties of 6016 aluminium alloy. Mater. Sci. Technol. **34**, 1511–1518 (2018). https://doi.org/10.1080/02670836.2018.1465514
15. W. Jiang, X. Chen, B. Wang, Z. Fan, H. Wu, Effects of vibration frequency on microstructure, mechanical properties, and fracture behavior of A356 aluminum alloy obtained by expendable pattern shell casting. Int. J. Adv. Manuf. Technol. **83**, 167–175 (2016). https://doi.org/10.1007/s00170-015-7586-0
16. W.Q. Zou, Z.G. Zhang, H. Yang, W. Li, Effect of vibration frequency on microstructure and performance of high chromium cast iron prepared by lost foam casting. China Foundry **13**, 248–255 (2016). https://doi.org/10.1007/s41230-016-6037-3
17. S. Kumar, S.P. Tewari, Metallurgical and mechanical characterization of A319 aluminum alloy casting solidified under mold oscillation. Int. Metalcast. **12**, 28–35 (2018). https://doi.org/10.1007/s40962-017-0135-x
18. M. Mehta, C.D. Mandal, S.K. Chaudhury, Microstructural changes and quality improvement of Al7Si0.2Mg (356) alloy by die vibration. Inter Metalcast **14**, 987–998 (2020). https://doi.org/10.1007/s40962-020-00408-3
19. V.S. Ayar, D.J. Gajjar, M.P. Sutaria, Effect of mechanical vibration on microstructure and mechanical properties of AlSi5Cu3 alloy. Int. Metalcast. **18**, 2415–2429 (2024). https://doi.org/10.1007/s40962-023-01179-3

20. H. Mu, Z. Wang, Z. Sun, B. Tang, B. Liu, W. Rao, Effects of ultrasonic vibration on the feeding behavior of AlSi(x)Mg0.35Cu0.6 alloy. Inter Metalcast (2026). https://doi.org/10.1007/s40962-026-01875-w
21. A.C. Kaya, M.E. Öztürk, A.G. Işık, İ Erdoğan, M.H. Sandık, Synthesizing of syntactic A356 foams using vibration-assisted gravity die casting. Int. Metalcast. **19**, 2928–2944 (2025). https://doi.org/10.1007/s40962-024-01518-y
22. S. Acar, K.A. Guler, A preliminary study upon the applicability of the direct water cooling with the lost foam casting process. Int. J. Metalcast. **15**, 88–97 (2021). https://doi.org/10.1007/s40962-020-00420-7
23. A. Kisasoz, K.A. Guler, A. Karaaslan, Influence of orbital shaking on microstructure and mechanical properties of A380 aluminium alloy produced by lost foam casting. Russ. J. Non-Ferrous Met. **58**, 238–243 (2017). https://doi.org/10.3103/s1067821217030063

Publisher's Note Springer Nature remains neutral with regard to jurisdictional claims in published maps and institutional affiliations.